THE ASTROPHYSICAL JOURNAL, 241:493–506, 1980 October 15

THE PHOTOMETRIC PROPERTIES OF BRIGHTEST CLUSTER GALAXIES. II. SIT AND CCD SURFACE PHOTOMETRY

J. G. HOESSEL
Palomar Observatory, California Institute of Technology
Received 1979 December 17; accepted 1980 April 22

ABSTRACT

Surface photometry of the first-ranked galaxy in 108 Abell clusters, obtained with SIT vidicon and CCD detectors, is presented. Galaxy structure, as parametrized by simple Hubble law models is found to correlate with galaxy absolute magnitude and cluster structure. All these structure data support and are interpreted on the dynamical friction evolution model. Twenty-eight percent of the galaxies have multiple component nuclei; the short lifetimes of such systems provide the best available evidence that ongoing evolution actually occurs. Average magnitude and structure evolution rates are derived from the data. When this result is combined with the expected rate of evolution of the stellar population in the galaxies, a corrected value of q_0 near the formal value is derived.

The correlation of absolute magnitudes and galaxy structure may be used to eliminate the magnitude dependence on cluster richness and Bautz-Morgan type and remove the effect of bias introduced into cluster samples by selection procedures. After removal of the trend due to differences in their evolution, the dispersion in the magnitudes of these brightest cluster galaxies is reduced to $\sigma = 0.21$ mag and the scatter in their core radii is 22% (1 σ).

Subject headings: cosmology — galaxies: clusters of — galaxies: photometry — galaxies: structure

I. INTRODUCTION

The remarkably small scatter in the absolute magnitudes of first-ranked cluster galaxies (e.g., Sandage 1972; Hoessel, Gunn, and Thuan 1980, hereafter cited as Paper I), which makes the Hubble diagram a powerful probe for observational cosmology, has been attributed to some special formation or evolutionary process (Sandage 1976; Dressler 1978*a*). One such process, the dynamical merger of cluster members to form the giant, has been the subject of considerable theoretical study (Ostriker and Tremaine 1975; White 1976; Gunn and Tinsley 1976, hereafter GT; Ostriker and Hausman 1977, hereafter OH; Hausman and Ostriker 1978, hereafter HO). Observational support for this model is available from the study of first-ranked galaxy structure (Oemler 1976), dynamics (Dressler 1979), and cluster luminosity functions (Dressler 1978*b*). A thorough understanding of its nature and the rate at which this process occurs is essential, since it generates a systematic evolution of the absolute luminosities of brightest cluster galaxies (GT), an effect which must be removed before meaningful results for the deceleration can be obtained.

The present work was undertaken in order better to understand the details of this evolutionary process and to calibrate its importance for observational cosmological methods. The theoretical results suggest that the dynamical-friction–induced cannibalism not only alters the luminosity of the brightest galaxy, but it also produces strong changes in the galaxy's structure (changing it from a normal elliptical galaxy to a cD system). Both luminosity and structure information are provided by the observational technique of surface photometry. To date, such data (detailed in § II) are available for the central regions of the brightest galaxies in 108 nearby Abell clusters, chosen randomly from the sample defined in Paper I. The structure data are parametrized by simple model galaxies; the results are listed and interpreted in § III. Implications of these results for cosmology are discussed in § IV. Future papers in this series will deal with the characteristics of the faint outer envelopes of brightest cluster galaxies and correlations of galaxy structure with cluster structure.

II. OBSERVATIONS AND REDUCTIONS

The majority of the surface-brightness observations reported here were obtained with a SIT vidicon area photometer at the 1.5 m Palomar telescope. Characteristics of this instrument are detailed by Kent (1979). The system produces a digital picture of 256×256 square pixels with 0.″55 separation. Several frames were obtained of each of the 108 galaxies. Generally 5 minute green and red exposures (on the system of Thuan and Gunn 1976) taken under photometric sky conditions were supplemented by two additional red frames with

integration times adjusted according to the galaxy's luminosity. In every case the noise due to sky photon statistics exceeded the instrumental noise.

Five relatively faint galaxies were observed with a CCD system (described by Young *et al.* 1978) at the prime focus of the 5 m Hale telescope. Ten minute exposures in both the green and red were obtained of the first-ranked galaxies in the clusters A166, A246, A274, A227, and A2328.

The raw picture data were reduced to multiaperture magnitudes by the following procedure: Zero-exposure erase frames taken throughout each night were subtracted from all other frames pixel by pixel. Dark emission during the short integrations used here is negligible in both instruments. Several flat-field exposures of a uniformly illuminated patch on the inside of the dome were made through the telescope in each color each night. Sky exposures were divided pixel by pixel by the averaged, normalized flat field of appropriate color. Prints of six red frames so treated are shown as Figure 1 (Plate 4). Sky background on each frame was determined by making a histogram of all pixels by data number and locating the peak value by a simple parabolic fit. This value was then subtracted from each pixel. The center of each object to be photometered was estimated by eye, then improved by an automated two-dimensional centering algorithm. Instrumental magnitudes were synthesized in circular apertures about this location.

Frames of system standard stars, obtained each night, were treated identically to the galaxy pictures. Root-mean-square residuals to the transformations to the standard star values were less than 0.04 mag for the SIT and 0.01 mag for the CCD. Galaxy magnitudes were reduced to outside the atmosphere utilizing these derived transformations. Further description of the absolute photometric results is the subject of Paper I.

Surface-brightness profiles, derived by differencing the multiaperture intensities, are shown in Figure 2 for six galaxies covering the range of observed size and shape in the sample. Throughout this paper all surface brightnesses are in units of red magnitudes per square arc second. Previous work on brightness profiles of luminous elliptical galaxies (e.g. Oemler 1976; Kormendy 1977) suggests that the interior regions may be adequately described by Hubble intensity laws. We choose to parametrize our observations by a modified Hubble law of the form

$$I(\gamma)=\frac{I_c}{1+\gamma^2/\beta^2}, \qquad (1)$$

where I_c is the central intensity, β the core radius, and γ the angular distance from the center. The luminosity contained within a projected radius γ is

$$L_\gamma=\pi I_c\beta^2\ln(1+\gamma^2/\beta^2), \qquad (2)$$

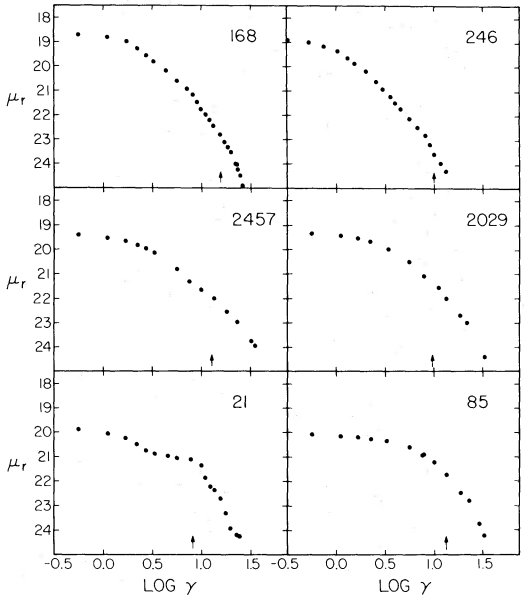

FIG. 2.—Red surface-brightness (in units of mag arcsec^{-2}) profiles for six galaxies in the sample (γ is angular radius in arc seconds). The arrow indicates the location of 16 kpc radial distance from the center. These objects were chosen to exhibit the range of characteristics observed in the entire sample. Final profiles extending to faint surface brightness for the entire sample will be published elsewhere.

yielding a magnitude of

$$m_\gamma=\mu_c-2.5\log[\pi\beta^2\ln(1+\gamma^2/\beta^2)], \qquad (3)$$

with μ_c denoting the central surface brightness. Standard nonlinear least-squares techniques were used to fit this relation to the multiaperture data for each object over the inner region of 16 kpc radius.

Profiles from three frames of the brightest galaxy in A2197, along with the averaged fit to these data, are illustrated in Figure 3. This object is more sharply cut off with increasing radius than the sample average, but is fitted somewhat better than average in the central region because of a favorable ratio of galaxy core radius to atmospheric seeing. Repeated observations during a single night yield fits which generally agree to 10% in core radius and 0.10 mag in μ_c. A later paper in this series will undertake detailed investigation of the profiles of the galaxies in this sample, extending the results to large radii and faint surface brightness. The complete profiles will be published therein.

Although the observations were made under relatively good atmospheric conditions, with the more distant objects measured in the best seeing, the core radius and central surface-brightness data are degraded by the atmosphere, telescope, and detector (at least for the SIT). To correct for this, all suitably bright stars were located on the pictures and multiaperture photometry

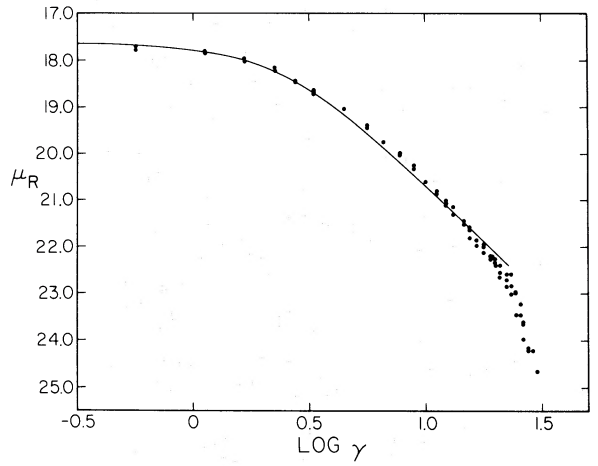

FIG. 3.—Average fit (*solid line*) to the observed profiles (points) for three red pictures of the brightest galaxy in A2197. The fit extends to 16 kpc metric radius.

obtained as above. Gaussian fits to these data provided knowledge of the run of image quality throughout each night. On average the image size was $\sigma(=\mathrm{FWHM}/2.35)=0\farcs7$ and ranged from $0\farcs3$ to $1\farcs0$.

In order to correct the core radius and central surface-brightness data for these degrading effects, artificial galaxy profiles were synthesized. A grid of synthetic galaxies was created by convolving Gaussians with the Hubble law (eq. [1]) and creating synthetic multiaperture magnitudes. These results were then fit with the same procedure as was used for the actual observations. The grid spacing used was $0\farcs1$ in both σ and β (true). The grid covered the full range of the parameters σ and β (observed). By locating these two values in the table the true core radius and the central surface-brightness correction ($\Delta\mu_c$) could be read off. Core radius corrections averaged less than 25%, with $\Delta\mu_c$ generally less than 0.30 mag. Twelve galaxies spanning the full range of core radii were observed on more than 1 night under differing atmospheric conditions. Comparison of the corrected core radii shows an rms scatter of 13% with a 0.18 mag scatter in μ_c. We adopt these values as the typical observational errors in these quantities. While this correction procedure is by no means optimal, it does not degrade the results of the present data appreciably.

Averaged corrected core radii from all frames of each object are listed in Table 1. Also listed are the average corrected central surface brightnesses. The final quantity in Table 1 is central surface brightness corrected for the galactic obscuration (as in Paper I) and corrected for the color change as a function of redshift, estimated from high-quality multichannel spectrometer data. The $(1+z)$ passband-stretching term, normally included in the K-correction, is not applied in Table 1 but will be accounted for below.

III. RESULTS

Observational data now available for the 108 brightest cluster galaxies include the core radius and central surface brightness from Table 1 and absolute magnitude, redshift, and the cluster properties of richness and Bautz-Morgan type (BM) from Table 1 of Paper I. In order to compare the properties of various galaxies and explore relationships between these properties we must eliminate the effects of the redshift and establish "absolute" quantities for each galaxy. A Hubble constant of $H_0=60$ km s^{-1} Mpc^{-1} and $q_0=\frac{1}{2}$ are assumed throughout the following. Each physical radius a, corresponding to the galaxy core radius β listed in Table 2, is derived from

$$a(\mathrm{kpc})=48.48\frac{\left[1-(1+z)^{-1/2}\right]}{1+z}\beta(\mathrm{arcsec}). \quad (4)$$

The mean core radius from these data is $\langle a\rangle=2.23\pm 0.1$ kpc with a dispersion of $\sigma_a=1.09$ kpc. Recalling that the observational uncertainty is 13% for this quantity, we find that this observed scatter is primarily cosmic.

A more convenient dimensionless parametrization of galaxy size is the power α used for the aperture correction by Gunn and Oke (1975, hereafter GO), i.e.,

$$L=L_s(\gamma/\gamma_s)^{\alpha}. \quad (5)$$

We term α the structure parameter in what follows. Rewriting this expression as

$$\alpha=\left(\frac{d\ln L}{d\ln\gamma}\right)_{\gamma_s}, \quad (6)$$

we find from equation (2) that

$$\alpha=\frac{2\gamma_s{}^2}{(1+\gamma_s{}^2/\beta^2)\beta^2\ln(1+\gamma_s{}^2/\beta^2)}, \quad (7)$$

where γ_s is our sampling radius corresponding to 16 kpc. The fourth column of Table 2 is a list of α values that are presented in a histogram in Figure 4. The mean of this distribution is $\langle\alpha\rangle=0.49\pm0.01$ with a dispersion of $\sigma_\alpha=0.11$. Observational uncertainties in β propagate to ±0.03 in α.

The final intrinsic parameter listed in Table 2 is the reduced surface brightness (RSB), which is the corrected central surface brightness of Table 1 further corrected for the fourth-power redshift dimming appropriate for any relativistic cosmology (Hubble and Tolman 1935). A histogram of the RSB data appears as Figure 5. The mean value is $\langle\mathrm{RSB}\rangle=18.13\pm0.06$ mag with a cosmic scatter of $\sigma_{\mathrm{RSB}}=0.62$ mag. These "mean galaxy" parameters are summarized in Table 3.

TABLE 1

OBSERVATIONAL DATA

Abell	β (arcsec)	μ_c (mu)	μ_c(A,K) (mu)	Abell	β (arcsec)	μ_c (mu)	μ_c(A,K) (mu)	Abell	β (arcsec)	μ_c (mu)	μ_c(A,K) (mu)	Abell	β (arcsec)	μ_c (mu)	μ_c(A,K) (mu)
21...	3.47	19.69	19.35	978...	1.14	17.84	17.65	1651...	1.63	19.06	18.88	2079...	1.73	18.56	18.42
76...	1.57	18.90	18.82	1020...	0.91	17.87	17.73	1691...	1.75	18.86	18.71	2092...	1.43	18.91	18.77
85...	5.72	19.99	19.87	1035...	1.18	18.46	18.29	1749...	1.27	17.96	17.84	2107...	2.95	18.88	18.79
104...	2.54	19.87	19.59	1126...	2.11	19.14	18.96	1767...	1.23	18.33	18.18	2124...	1.60	18.79	18.65
119...	2.20	18.58	18.48	1139...	1.21	17.89	17.81	1773...	1.28	18.51	18.34	2142...	1.69	19.62	19.42
147...	2.04	18.86	18.77	1185...	4.03	18.94	18.87	1775...	1.05	17.97	17.82	2147...	2.49	18.60	18.47
151...	2.06	18.31	18.20	1187...	1.38	18.61	18.44	1793...	0.90	18.59	18.41	2151...	2.20	18.26	18.13
154...	1.33	18.16	17.99	1213...	1.05	17.55	17.45	1795...	2.04	18.94	18.80	2152...	1.28	17.92	17.78
166...	0.94	19.51	19.26	1216...	0.97	18.03	17.92	1809...	1.33	18.42	18.25	2162...	1.51	17.48	17.37
168...	1.55	18.19	18.09	1228...	1.01	17.43	17.36	1831...	1.52	18.58	18.42	2175...	1.39	19.06	18.80
189...	1.24	17.58	17.51	1238...	0.97	18.28	18.12	1904...	1.35	18.24	18.09	2197...	2.10	17.38	17.26
193...	1.62	17.66	17.56	1254...	1.16	18.33	18.15	1913...	1.38	18.70	18.59	2199...	4.57	18.66	18.53
194...	1.60	16.92	16.88	1291...	1.67	19.25	19.12	1927...	1.85	19.51	19.35	2255...	0.99	18.07	17.78
225...	1.38	18.68	18.46	1318...	1.41	16.89	16.85	1983...	0.85	17.67	17.57	2256...	2.51	18.50	18.20
246...	0.94	18.40	18.25	1364...	0.92	18.71	18.48	1991...	2.23	19.04	18.91	2328...	0.98	19.11	18.67
274...	1.21	19.25	18.98	1365...	1.12	18.44	18.28	1999...	1.82	19.47	19.25	2347...	1.16	19.25	18.94
277...	1.22	18.92	18.72	1367...	1.99	17.30	17.26	2005...	1.54	19.60	19.33	2382...	1.98	19.29	19.15
389...	2.01	19.79	19.54	1377...	0.94	17.57	17.46	2022...	1.43	18.24	18.12	2384...	1.93	19.70	19.50
399...	2.64	19.87	19.62	1382...	1.58	19.25	18.98	2028...	1.12	18.24	18.07	2399...	0.69	17.49	17.31
400...	0.97	16.60	16.55	1399...	1.16	19.06	18.86	2029...	2.94	19.09	18.92	2410...	1.49	18.90	18.73
401...	1.71	19.03	18.77	1412...	2.12	19.92	19.69	2040...	1.13	18.15	18.05	2457...	1.67	18.36	18.23
496...	2.64	18.31	18.11	1436...	1.22	18.35	18.21	2048...	1.29	18.47	18.27	2634...	1.99	17.85	17.62
500...	1.18	18.27	18.03	1468...	1.05	18.77	18.59	2052...	2.87	18.90	18.82	2657...	1.98	19.26	19.17
634...	2.31	18.26	17.94	1474...	1.05	18.96	18.79	2061...	1.25	18.20	18.03	2666...	2.16	17.58	17.37
671...	2.00	18.33	18.07	1496...	1.27	19.54	19.33	2063...	2.75	18.83	18.76	2670...	1.16	18.15	17.99
779...	2.31	17.33	17.24	1541...	1.16	18.62	18.43	2065...	1.77	19.17	19.02	2675...	1.49	18.88	18.72
957...	1.65	18.03	17.87	1644...	2.68	19.02	18.88	2067...	0.99	18.67	18.51	2700...	1.32	18.99	18.78

TABLE 2

INTRINSIC PROPERTIES OF GALAXIES

Abell	M_{VI}	a(kpc)	α	RSB(mu)	Abell	M_{VI}	a(kpc)	α	RSB(mu)	Abell	M_{VI}	a(kpc)	α	RSB(mu)
21...	-23.30	6.80	0.90	18.94	1228...	-22.14	0.76	0.33	17.22	2028...	-22.92	1.84	0.45	17.75
76...	-22.61	1.34	0.40	18.66	1238...	-22.49	1.49	0.42	17.82	2029...	-23.43	4.86	0.74	18.60
85...	-22.98	7.01	0.92	19.64	1254...	-22.49	1.59	0.43	17.88	2040...	-22.07	1.16	0.38	17.86
104...	-22.76	4.41	0.70	19.25	1291...	-21.97	2.15	0.49	18.88	2048...	-22.94	2.52	0.52	17.88
119...	-22.71	2.20	0.49	18.29	1318...	-21.96	0.63	0.31	16.77	2052...	-22.50	2.30	0.50	18.67
147...	-22.23	2.02	0.47	18.59	1364...	-22.71	2.00	0.47	18.04	2061...	-23.09	2.08	0.48	17.71
151...	-23.15	2.40	0.51	17.97	1365...	-22.58	1.82	0.45	17.96	2063...	-22.45	2.12	0.48	18.61
154...	-23.01	1.78	0.45	17.73	1367...	-22.38	0.95	0.35	17.17	2065...	-22.59	2.74	0.55	18.71
166...	-22.28	2.17	0.49	18.79	1377...	-22.52	1.06	0.37	17.25	2067...	-22.23	1.54	0.42	18.21
168...	-22.54	1.59	0.43	17.90	1382...	-22.86	3.37	0.61	18.54	2079...	-22.97	2.46	0.52	18.14
189...	-22.05	0.99	0.36	17.36	1399...	-22.37	2.20	0.49	18.48	2092...	-22.31	2.07	0.48	18.49
193...	-22.84	1.73	0.44	17.35	1412...	-22.39	3.74	0.64	19.34	2107...	-22.84	2.80	0.55	18.61
194...	-22.83	0.67	0.31	16.81	1436...	-22.73	1.71	0.44	17.94	2124...	-22.87	2.32	0.50	18.36
225...	-22.69	2.06	0.48	18.17	1468...	-22.50	1.88	0.46	18.23	2142...	-22.46	3.20	0.59	19.05
246...	-22.18	1.51	0.42	17.93	1474...	-22.11	1.74	0.44	18.47	2147...	-22.59	2.13	0.49	18.31
274...	-22.97	3.04	0.58	18.45	1496...	-22.37	2.52	0.52	18.94	2151...	-22.55	1.80	0.45	17.98
277...	-22.85	2.39	0.51	18.32	1541...	-22.81	2.16	0.49	18.06	2152...	-22.45	1.27	0.39	17.59
389...	-22.95	4.66	0.72	19.06	1644...	-22.55	2.74	0.55	18.69	2162...	-22.55	1.10	0.37	17.24
399...	-22.66	4.10	0.67	19.32	1651...	-22.87	2.89	0.56	18.53	2175...	-22.74	2.80	0.55	18.40
400...	-22.16	0.52	0.29	16.45	1691...	-22.94	2.71	0.54	18.40	2197...	-23.08	1.46	0.41	17.13
401...	-22.82	2.75	0.55	18.45	1749...	-22.86	1.57	0.43	17.60	2199...	-23.25	3.28	0.60	18.40
496...	-22.71	1.97	0.47	17.97	1767...	-22.86	1.88	0.46	17.88	2255...	-22.92	1.58	0.36	17.47
500...	-22.74	1.70	0.44	17.75	1773...	-22.91	2.11	0.48	18.02	2256...	-23.30	3.05	0.58	17.97
634...	-22.35	1.42	0.41	17.93	1775...	-22.88	1.62	0.43	17.52	2328...	-23.37	2.65	0.54	18.10
671...	-23.10	2.21	0.49	17.86	1793...	-22.51	1.61	0.43	18.05	2347...	-22.73	2.76	0.55	18.45
779...	-22.92	1.09	0.37	17.15	1795...	-22.79	2.80	0.55	18.54	2382...	-22.37	2.79	0.55	18.88
957...	-22.91	1.62	0.43	17.68	1809...	-23.12	2.22	0.49	17.92	2384...	-22.51	3.77	0.64	19.11
978...	-22.78	1.33	0.40	17.42	1831...	-23.04	2.43	0.52	18.11	2399...	-22.38	0.89	0.34	17.07
1020...	-22.16	1.28	0.39	17.46	1904...	-23.12	2.08	0.48	17.78	2410...	-22.88	2.54	0.53	18.39
1035...	-22.88	2.00	0.47	17.95	1913...	-22.33	1.63	0.43	18.36	2457...	-22.86	2.18	0.49	17.98
1126...	-23.16	3.68	0.64	18.62	1927...	-22.36	2.93	0.56	19.04	2634...	-22.91	1.44	0.41	17.49
1139...	-22.14	1.03	0.36	17.65	1983...	-21.99	0.87	0.34	17.38	2657...	-21.68	1.85	0.46	19.00
1185...	-22.80	3.21	0.59	18.72	1991...	-22.64	2.88	0.56	18.67	2666...	-23.11	1.36	0.40	17.25
1187...	-22.88	2.32	0.59	18.11	1999...	-22.84	3.83	0.65	18.82	2670...	-23.00	1.91	0.46	17.68
1213...	-22.69	1.13	0.38	17.24	2005...	-22.91	3.80	0.65	18.82	2675...	-22.61	2.32	0.50	18.42
1216...	-22.18	1.13	0.38	17.70	2022...	-22.62	1.78	0.45	17.88	2700...	-22.86	2.66	0.54	18.38

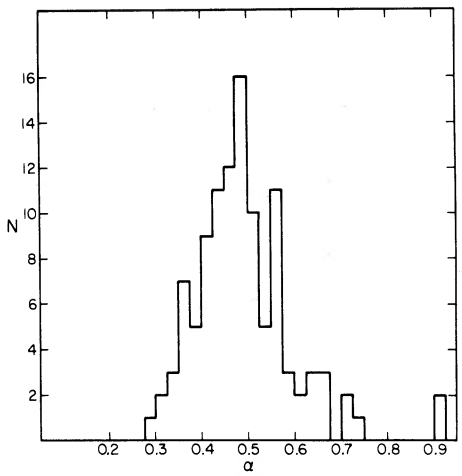

FIG. 4.—Histogram of the dimensionless structure parameters for the 108 galaxies in the sample. The mean of this distribution is $\langle\alpha\rangle = 0.49$ with the dispersion $\sigma_\alpha = 0.11$.

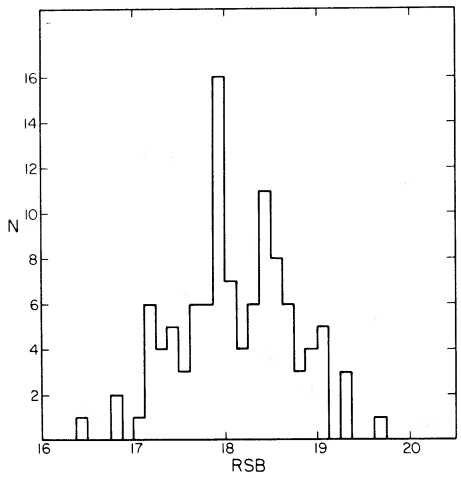

FIG. 5.—Histogram of reduced central surface brightness for the galaxies in the sample. The mean is $\langle RSB\rangle = 18.13$ mag with dispersion $\sigma_{RSB} = 0.62$ mag.

TABLE 3

SUMMARY OF MEAN GALAXY PROPERTIES

Quantity	Mean	σ
M_{VI}.....	-22.68 ± 0.03 mag	0.35
log a	$+0.30$	0.20
α	$+0.49 \pm 0.01$	0.11
RSB.....	$+18.13 \pm 0.06$ mag	0.62

A result of Paper I (and earlier work; see, e.g., Kristian, Sandage, and Westphal 1978) is that the absolute magnitudes of first-ranked galaxies are correlated with the cluster properties of richness and BM type. We find that the brightest galaxy structure is also correlated with these properties. In Figure 6 the structure parameter histogram is subdivided by Abell richness class. Mean values for each class are given in Table 4. Although the sample suffers from a lack of rich clusters, an increase in the mean alpha of 0.06 per class is shown by the data. A weak correlation between structure parameter and cluster BM type is shown in Figure 7. Means for each class are listed in Table 5. These correlations are consistent with the predictions of the dynamical-friction galaxy-evolution model in which the BM sequence is interpreted as a result of differing degrees of evolution with the type I clusters being highly evolved. The structure parameter increases in this model as the cannibal dines on its neighbors and grows in luminosity at their expense, which happens at a faster rate in richer, denser systems (see GT or HO).

TABLE 4

MEAN STRUCTURE PARAMETER BY RICHNESS CLASS

Richness	$\langle\alpha\rangle$	σ
0.....	0.41 ± 0.02	0.06
1.....	0.49 ± 0.01	0.11
2.....	0.54 ± 0.03	0.11
3.....	0.52	...

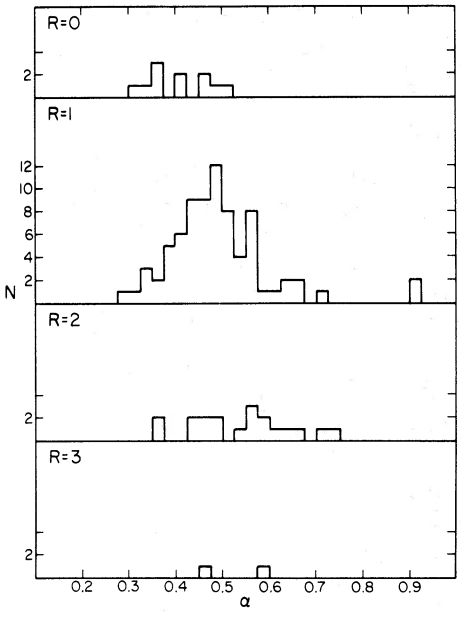

FIG. 6.—Histogram of structure parameter data for each Abell richness class. Mean alphas for each class are listed in Table 4.

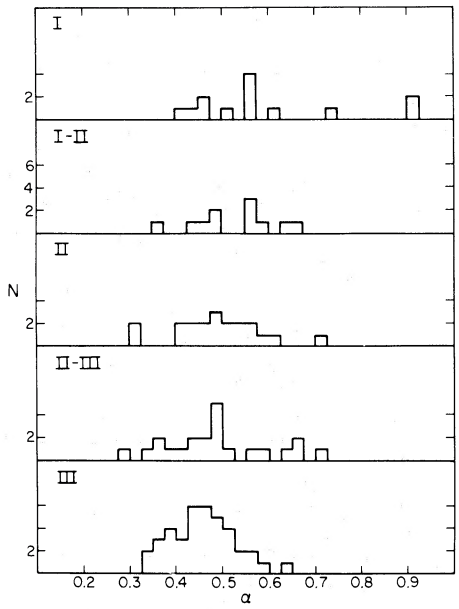

FIG. 7.—Histogram of structure class for each cluster Bautz-Morgan type. Mean alphas for each type are listed in Table 5.

TABLE 5

MEAN STRUCTURE PARAMETER BY BAUTZ-MORGAN TYPE

BM	⟨α⟩	σ
I.....	0.59±0.05	0.17
I–II.....	0.52±0.03	0.09
II.....	0.50±0.02	0.10
II–III.....	0.47±0.02	0.11
III.....	0.47±0.01	0.07

This dynamical evolution introduces important errors into the global Hubble-diagram method of deceleration measurement. As stressed by GT, the aperture magnitudes of galaxies change with time, an effect which must be calibrated before meaningful results for q_0 may be obtained. Another serious problem is that selection procedures tend to find mainly rich, dense clusters at the faintest levels, and this correlation of galaxy and cluster properties introduces the well-known Scott (1957) effect. Is there any way of eliminating these problems? One possibility suggested by HO is the expected correlation of structure and absolute magnitude. Absolute intrinsic magnitudes from Table 2 are plotted against α in Figure 8. The observational uncertainties are shown in the lower right. Evolutionary tracks in this plane are calculated by HO. The data are replotted in Figure 9 where the points are average value in bins of 0.05 for α less than 0.5, and bins of 0.10 for α in excess of 0.5. The error bars represent $\pm 1\ \sigma$ dispersions in the data, where the uncertainty in the mean value is illustrated at the lower right. The dispersion of

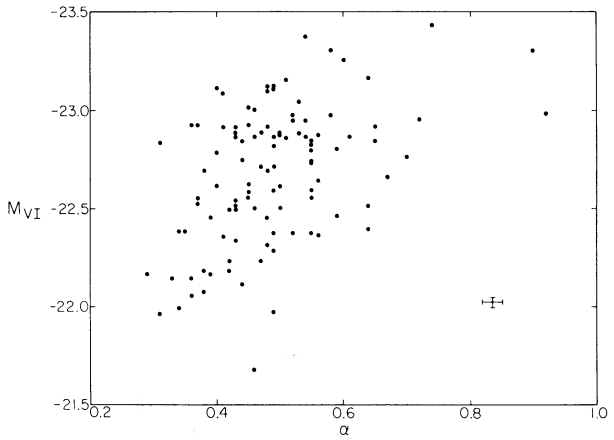

FIG. 8.—Absolute intrinsic magnitudes in a 16 kpc radius aperture are plotted against structure parameter for the sample galaxies. The error bars at the lower right illustrate the observational uncertainty in each point.

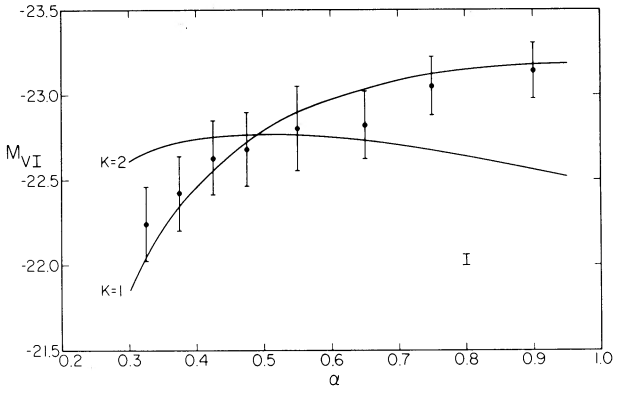

FIG. 9.—The data of Fig. 8 are replotted as mean absolute magnitudes in bins of structure parameter. The error bars represent the dispersions in the data. Errors in the determination of the mean points are shown at the lower right. As explained in the text the solid curves are the theoretically expected loci for two different rates of galaxy core growth with accreted mass.

the data about the mean line is $\sigma=0.22$ mag, and it decreases somewhat from left to right, consistent with the prediction of HO. This observed scatter is somewhat less than anticipated by HO.

In order to study this process in more detail, let us assume, following GT, that in a merger the galaxy scale size (a) increases as the kth power of the mass (m); that is if

$$\frac{\delta a}{a} = k\frac{\delta m}{m}, \tag{8}$$

then

$$\frac{\delta L}{L} = \frac{\delta m}{m}(1-k\alpha), \tag{9}$$

if the accreted material has the same mass-to-light ratio as the original (GT eq. [17]). Taking $\chi=\beta/\gamma_s$, we derive

$$\frac{\delta L}{L}=\left(\frac{1}{k}-\alpha\right)\frac{\delta\chi}{\chi}, \tag{10}$$

which may be integrated to obtain

$$L_s=c'\chi^{1/k}\ln(1+1/\chi^2), \tag{11}$$

or

$$M_s=-2.5\log\left[\chi^{1/k}\ln(1+1/\chi^2)\right]+c. \tag{12}$$

This relation, along with equation (7) may be used to find the expected behavior in the (M_{VI}, α)-plane for various values of k. Two such loci are shown in Figure 9 for $k=1$ and $k=2$, having been vertically adjusted to fit the data at $\alpha=0.49$. The case $k=1$ is the expected behavior (GT) for the homologous merger of galaxies of nearly the same size, whereas $k=2$ is expected for large objects consuming small ones. The data are remarkably well fitted by the $k=1$ case. HO have suggested relatively large objects located near the cannibal to be its most likely victims, i.e., those with the shortest relaxation times, which is consistent with this observed behavior and the large luminosity difference between the first- and second-ranked galaxies in highly evolved (Bautz-Morgan type I) systems (Sandage and Hardy 1973).

Absolute magnitudes and structure parameters are plotted as functions of cluster redshift in Figure 10. A trend in the data toward larger, more luminous galaxies with increasing distance in the sample is apparent. This effect is too large to be easily explained by incorrect choice of q_0 (a value 6 σ away from the formal result of Paper I is necessary to explain the data). An alternate hypothesis is that a selection effect exists in the distance-class–limited sample. Atypical clusters containing larger, more luminous brightest galaxies than average are included in the sample, particularly at the largest redshifts which are beyond the completeness limit ($z\approx0.06$) of the sample. Applying a statistical correction to the absolute magnitudes based on the measured values of α for each galaxy and the mean line defined by the data in Figure 9 eliminates this dependence of absolute magnitude on redshift. It appears that this "α-correction" may be used to correct for the

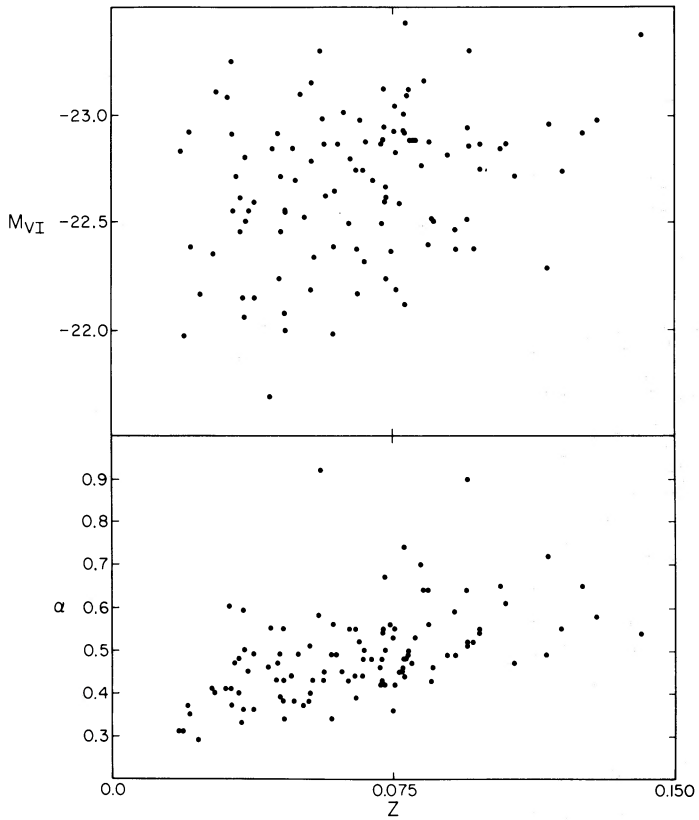

FIG. 10.—Correlations of intrinsic absolute magnitude (*upper panel*) and structure parameter (*lower panel*) with redshift for galaxies in the sample. Interpreted as selection bias in the distance-class limited sample, the trend of increasing absolute brightness with redshift is eliminated if the data are corrected via the mean $(M_{VI}-\alpha)$ relation (shown in Fig. 9).

effects of selection bias in cluster samples and thereby eliminate the Scott effect. Alpha corrections, applied throughout the remainder of this paper, have as their zero points the mean values of $\langle\alpha\rangle = 0.49$ and $\langle M_{VI}\rangle = -22.68$.

During the course of obtaining the redshifts for the clusters in this sample it was noticed that a sizable fraction of the first-ranked galaxies have multiple nuclei. This is often not apparent on Schmidt prints (or plates) because of excessive density and insufficient scale. A small subset of these objects are the binary objects studied by Rood and Leir (1979). In order to determine the fraction of multiple systems and isolate individuals for further study, a photographic survey of the sample on short-exposure large-scale plates was undertaken with the 2.5 m Hooker and the 1.5 m Palomar telescopes. Halfway through this project the SIT system became available and was used to complete the survey. One well-known multiple system, in A2199, is shown in Figure 1. All galaxies in the sample with multiple components separated by less than 16 kpc are listed in Table 6. Two of these clusters, A88 and A1656 are not included in the discussion below for lack of sufficient surface photometry. Two objects, in A2199 and A21, are triple systems. Thirty-three sample galaxies are multiple—a fraction of 28%. A sizable number of such systems are expected to form during dynamical evolution (GT, HO). Close collisions (of less than 16 kpc impact parameter) between cluster members and the brightest galaxy are expected every 10^9 yr for the typical sample cluster (Bahcall 1977). Simulations of the merger process (e.g., White 1978) indicate that the actual merger takes approximately one orbital time ($\sim 2.5 \times 10^8$ yr in this case). Thus the observed fraction of multiple systems is consistent with the expected frequency if all merges result in a detectable multiple system at some stage.

The time since cluster collapse for the typical cluster in the present sample if $4-5 \times 10^9$ yr (Gunn and Gott 1972). Thus we expect approximately four mergers to have occurred. The mean absolute magnitude of the multiple systems is 0.12 brighter than that of the nonmultiple galaxies. The mean structure parameter for the multiples is 0.05 larger than the single-component systems. If we assume these changes to be typical for the accretion of a galaxy, we can crudely estimate that the average sample galaxy was formerly four individuals; both from the magnitude and α differences between the "mean" galaxy at $\alpha = 0.30$, which are presumed to be in the primordial state.

One more observed relationship supports the dynamical evolution model. Reduced surface brightness and structure parameters are plotted in Figure 11. Typical observational error is also shown. The dispersion of the RSB data about the mean relation defined by the data is $\sigma = 0.23$ mag; approximately half of the variance can be accounted for by the observational uncertainties. For the simple homologous merger of N objects to form a giant (i.e., the $k = 1$ case above) the central surface brightness is expected to decrease like $1/N$ (see OH). The average sample galaxy RSB = 18.13 mag, which is a factor of 4 down from the RSB of the smallest, least-luminous galaxies in the sample. This result provides independent confirmation that approximately four objects have on average merged to create the first-ranked galaxy. To summarize, the observational results discussed in this section are all entirely consistent with dynamical merger of galaxies in clusters. The high frequency of multiple nucleus systems is difficult to explain without such evolution.

TABLE 6

CLUSTERS WITH MULTIPLE-COMPONENT BRIGHTEST GALAXIES

Abell	Abell	Abell
21	779	2067
88	1126	2092
104	1185	2142
151	1291	2151
154	1468	2175
193	1496	2199
194	1656	2256
277	1927	2328
389	1991	2384
400	2052	2410
671	2063	2634

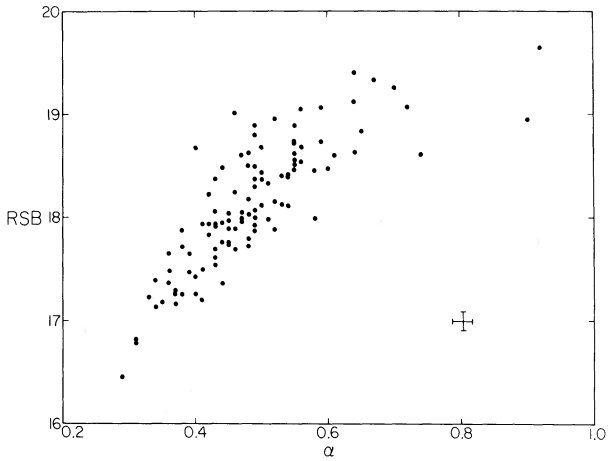

FIG. 11.—Reduced central surface brightness is plotted as a function of galaxy structure parameter for the data (from Table 2). Observational uncertainties appropriate for each point are illustrated at the lower right. Dispersion of the surface-brightness data about the mean (RSB − α) relation defined by the data is $\sigma = 0.23$ mag.

IV. DISCUSSION

This evolution of the brightness and structure of brightest galaxies has important consequences for ob-

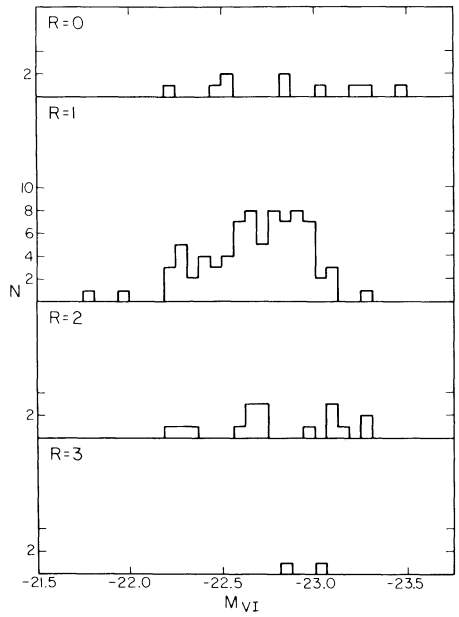

FIG. 12.— Alpha-corrected absolute magnitudes are histogrammed for each cluster richness class. The clear trend of brighter brightest galaxies in richer clusters (Paper I) has been eliminated by the alpha correction.

servational cosmology, particularly its influence on the values of the deceleration obtained from global methods. Is the α correction all that is necessary to eliminate this systematic effect, or are the corrected magnitudes still correlated with other properties, such as cluster richness or BM type? Alpha-corrected absolute magnitudes are presented in a histogram in Figure 12 by richness class. Mean absolute magnitudes for each class are listed in Table 7. The clear trend toward brighter galaxies in richer clusters, shown in Figure 2 of Paper I for these data, has all but disappeared. Corrected magnitudes binned by BM type are shown in Figure 13, and the mean values tabulated in Table 8. Again the trend found in Paper I has been eliminated. Richness plus BM corrections for each galaxy are plotted against the α correction in Figure 14. We believe the α correction, which reduces the dispersion in the magnitudes of first-ranked galaxies to $\sigma = 0.21$ mag, is the more fundamental method, richness and BM magnitude trends being due to correlation of galaxy structure with these cluster properties. The results shown in Figure 14 suggest that the richness and BM corrections cannot properly eliminate the evolution, particularly for nearly primordial (i.e., $\alpha \approx 0.3$) objects. Work in progress will determine if other cluster properties, such as the form of the luminosity function or the central number density of galaxies may be used in place of the α correction (see HO).

For faint high-redshift clusters the quantity α is not impossible to measure (since 16 kpc corresponds to 2.″5

TABLE 7

MEAN ABSOLUTE MAGNITUDES AFTER ALPHA-CORRECTION

Richness	$\langle M_{VI}(\alpha) \rangle$	σ
0.....	-22.80 ± 0.13	0.40
1.....	-22.63 ± 0.03	0.28
2.....	-22.75 ± 0.08	0.33
3.....	-22.88	...

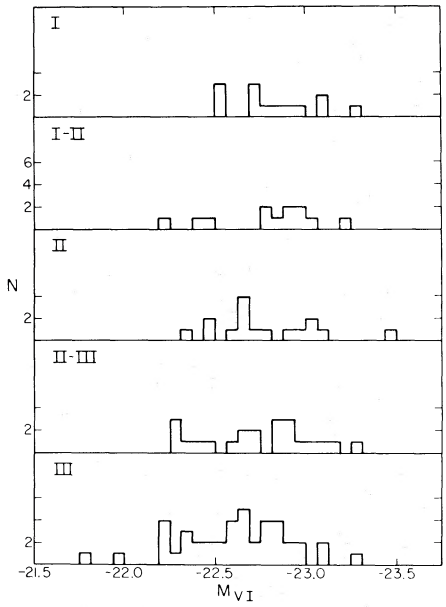

FIG. 13.— Alpha-corrected absolute magnitudes are histogrammed for each cluster Bautz-Morgan type. The trend found in the uncorrected data shown in Fig. 3 of Paper I is reduced to less than statistically significant by the alpha correction.

TABLE 8

MEAN ABSOLUTE MAGNITUDES AFTER ALPHA-CORRECTION

BM	$\langle M_{VI}(\alpha) \rangle$	σ
I.....	-22.70 ± 0.07	0.24
I–II....	-22.76 ± 0.10	0.31
II.....	-22.75 ± 0.07	0.28
II–III...	-22.70 ± 0.06	0.30
III.....	-22.56 ± 0.05	0.30

at $z = 0.6$), but it will not be easy. Also, in order to measure α, q_0 must be known. An iterative procedure may be used to solve for q_0 with the Hubble diagram; α=corrections calculated for some initial q_0 are applied and a new q_0 derived; then the procedure is repeated until it converges. Since intrinsically brighter galaxies are larger and an incorrect value of q_0 results in an error of the same sign, i.e., too large a q_0 corresponds to brighter, larger-angular-size galaxies, the

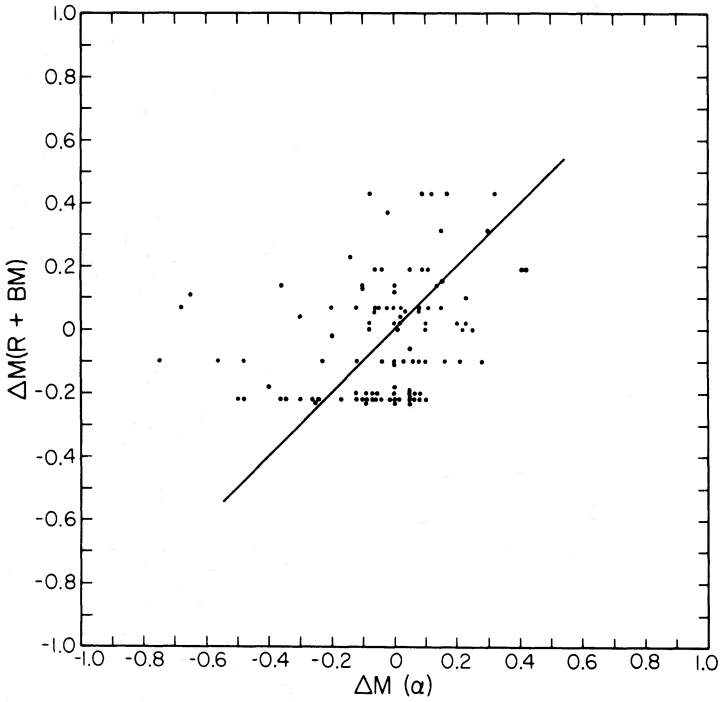

FIG. 14.—Richness plus Bautz-Morgan corrections derived from the data of Paper I are plotted against the alpha corrections for each galaxy in the sample. Perfect correlation is illustrated by the line. The ΔM(R + BM [combined richness and Bautz-Morgan effects]) appears to fail, particularly for systems with small (nearly primordial) core radii.

α-correction reduces the sensitivity of the Hubble diagram to q_0. This reduction in sensitivity is of the same order as the gains from the reduced dispersion the correction provides. If some property of the cluster, independent of q_0, can be found to correlate well with the evolutionary state of the brightest galaxy, this sensitivity reduction may be avoided.

If at present we ignore selection bias in the data used for the Hubble diagram (Fig. 4 of Paper I), we can estimate the influence of dynamical evolution on that result. The time between the epoch of the faint clusters ($z \approx 0.3$) and the epoch of the bright clusters ($z \approx 0.07$) corresponds to consumption of two or three galaxies by the cannibal. At $\Delta = 0.12$ mag per event, a correction to the formal value of q_0 in the range $1 < \Delta q_0 < 1.7$ in the sense q_0 (true) $= q_0$ (formal) $+ \Delta q_0$ is necessary. A similar correction of opposite sign is the best available estimate for the influence of the evolution of the stellar populations in the galaxies (Tinsley and Gunn 1976, hereafter TG). Thus the true deceleration is probably near the formal value, in the absence of selection bias in the sample used.

Clusters richer on average than the low-redshift sample are preferentially selected at large distances; thus the dynamical evolutionary correction is somewhat offset by selection. A quantitative estimate of the magnitude of this effect cannot yet be made.

The deviation from the $1/(1+z)^4$ behavior of central surface brightness with redshift has been proposed as a means of measuring the rate of stellar evolution in galaxies (Gudehus 1975; Petrosian 1976; Tinsley 1976). The large dispersion introduced by dynamical evolution of the central surface brightness, as well as the systematic trend with redshift and selection bias, combine to render raw central surface brightness useless for this purpose. Measurement of the structure parameter may be used to eliminate these problems, via the relationship shown in Figure 11, with the price that the surface brightness–redshift effect is no longer independent of cosmological model. Alpha-corrected central surface brightness is plotted as a function of $\log(1+z)$ in Figure 15. The scatter in the data is large, but a correlation does exist with a best-fit slope of 13.7 ± 2.8, slightly over 1 σ from the expected slope of 10 for no evolution. It has long been realized that this plot can provide a fundamental direct test for the expansion of the universe (Hubble and Tolman 1935; Geller and Peebles 1972). Tired-light cosmologies, where the change in energy per photon with redshift is the only effect, have a slope in this plane of 2.5, which is 4 σ from the observations.

Assuming the absence of strong radial gradients, the stellar evolution of central surface brightness is (following GO):

$$\delta \mathrm{SB} = (1.3 - 0.3x) \ln t_1/t_0, \qquad (13)$$

where x is defined for the stellar mass (m_s) function in

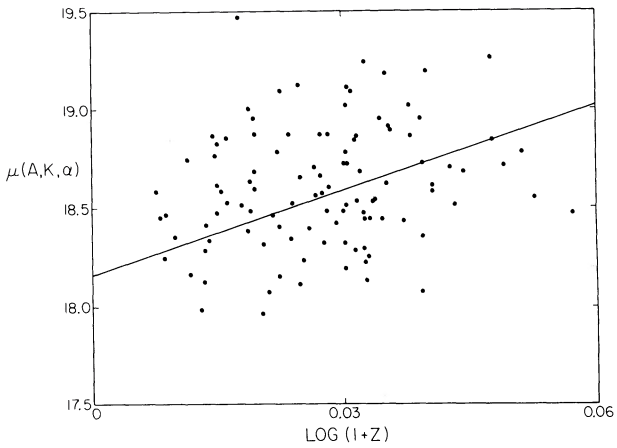

FIG. 15.—Totally corrected central surface brightness is plotted as a function of $\log(1+z)$. The best-fit line has a slope of 13.7 ± 2.8. In the absense of stellar evolution a slope of 10 is expected for all relativistic cosmologies. Tired light universes (slope 2.5) are inconsistent with these data.

a galaxy by

$$\frac{dN}{dm_s} = Cm_s^{-(1+x)}. \quad (14)$$

For $q_0 = 1/2$ (where $t_1/t_0 = (1)/[(1+z)^{3/2}]$) and $x = 1$ (see TG), we list expected δSB's for several redshifts in Table 9. The slope error for the data in Figure 15 corresponds to 0.10 mag at $z = 0.07$ where most of our data are. Thus the data lie 2σ away from the expected line, including evolution. Improved measurements can make sizable improvements in the significance of this sort of result, since half the slope error may be attributed to the present observational uncertainties. Careful extension of these data to larger distances is necessary before actual estimates of the evolution rate may be obtained. If the slope of the surface brightness–redshift relation continues to exceed 10, the extra complication of intergalactic extinction may have to be faced (Gudehus 1975).

An alternate global test using galaxies is the metric diameter-redshift relation. Baum (1972) has applied this method using a clever photographic technique. Others have suggested core radii for first-ranked galaxies to be good metric rods, independent of the stellar evolution (Petrosian 1976; Tinsley 1976). A core radius–redshift plot for our data is shown in Figure 16, along with the expected behavior for $q_0 = 0$ and $q_0 = 1$. (See, e.g., Sandage 1961 for theory.) The separation between these models amounts to 30% at $z = 0.6$. The cosmic dispersion in core radii is $\sim$50% which, along with the systematic dynamical evolution of the core radii, makes this method less than attractive. Also faint cluster samples are biased toward larger galaxies, as discussed § III.

The correlation between core radius and central surface brightness may be used to reduce this dispersion and eliminate the systematic trends. The core radius–RSB relation is shown in Figure 17. Elimination of the systematic trend reduces the observed core-radius dispersion to $\sigma_a = 22\%$; half of this variance corresponds to the observational uncertainties. Figure 18 illustrates the core radius–redshift data, after a correction based on the empirical relationship shown in Figure 17 and the measured RSB for each galaxy has been applied. This procedure tightens the radius-redshift data considerably, and the method promises to be a powerful cosmological test if accurate rates for the stellar evolution of central surface brightness become available, in order to enable the RSB–radius correction to be applied at high redshift. From the ground, the core-radius measurements for high-redshift clusters are difficult at best, but the Space Telescope will have sufficient sensitivity and resolution to measure directly both the core radius and central surface brightness at any redshift.

Resolving the entanglement of deceleration and evolution will be difficult if only magnitudes, core radii, central surface brightnesses, and redshifts are available. Incorrect estimation of the stellar evolution

TABLE 9

STELLAR EVOLUTIONARY SURFACE-BRIGHTNESS CHANGES FOR $x = 1$

z	δSB (mag per arcsec^2)
0.07...	0.10
0.15...	0.21
0.30...	0.39
0.60...	0.70

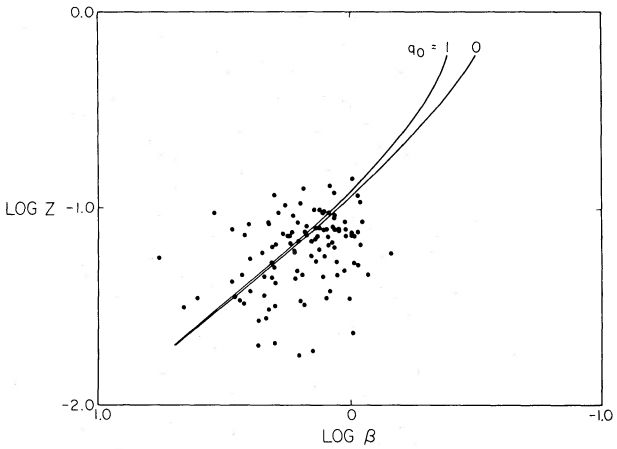

FIG. 16.—The core radius–redshift diagram has been proposed as a cosmological test. The large dispersion and systematic bias in the raw core-radius data for any cluster sample combine to make this method less than promising.

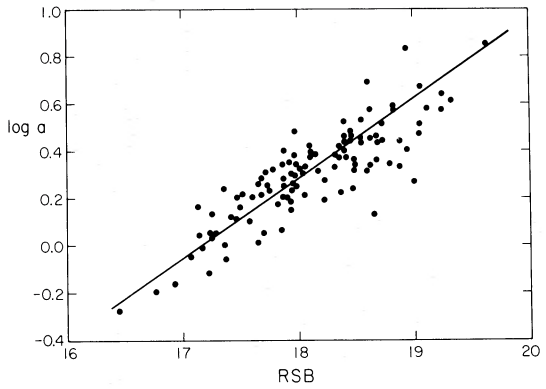

FIG. 17.—Galaxy core radii are plotted against central surface brightness. A relation of the form $RSB = 2.93 \log a + 17.15$ fits the data well. This relation also holds for lower absolute-luminosity ellipticals in the Virgo cluster (Kormendy 1977).

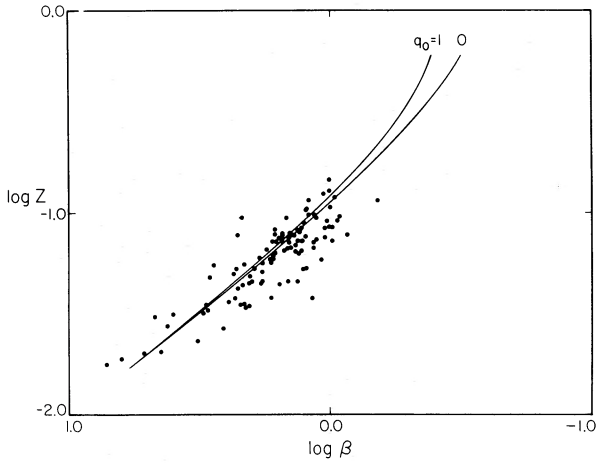

FIG. 18.—The core radii plotted in this figure have been corrected on the basis of the empirical relationship shown as Fig. 17 and the measured RSB for each galaxy. This method is then corrected for the systematic influence of dynamical evolution and promises to be a sensitive cosmological test.

rates results in q_0 error of the same sign for both the Hubble diagram and metric diameter tests. The magnitude of the errors is, however, not identical for the two methods; only the correct stellar evolution rate should result in the same deceleration being determined from both techniques. It remains to be seen whether all other systematic effects can be eliminated to the extent that this becomes practical.

The mean surface brightness–core radius relation defined by the data shown in Figure 17 may be written as

$$RSB = 2.93 \log a + 17.15. \quad (15)$$

This is identical to the relation found by Kormendy (1977) (after accounting for photometric system differences and the definition of core radius), largely from King's (1978) photometry of Virgo cluster ellipticals of considerably lower absolute luminosity than the present sample. Acceptance of the evolutionary cause for this relation for the first-ranked galaxies hints that a physically similar process, i.e., the homologous merger of small systems to form larger ones, may be important in the formation of all elliptical galaxies. Accurate surface photometry of a large sample of galaxies extending deep into the cluster luminosity function to check this result is necessary and could provide an important clue for the detailed understanding of the galaxy formation process.

V. SUMMARY

Surface photometric observations of the brightest galaxies in 108 Abell clusters lead to several conclusions relevant to observational cosmology.

1. All available evidence indicates that dynamical friction strongly affects the structure and luminosity of first-ranked galaxies.

2. Galaxy structure is correlated with the cluster properties of richness and Bautz-Morgan effects.

3. Galaxy absolute magnitude is correlated with structure. An observed relation may be used to eliminate the dependence of absolute magnitude on cluster properties, minimize the dispersion in magnitude to $\sigma = 0.21$ mag, and remove the systematic trend of dynamical evolution.

4. The average nearby Abell cluster has had four members combine to form the giant which grows in aperture luminosity by 0.12 mag for each capture, which happens with a time scale of $\sim 10^9$ yr.

5. This rate implies a correction in the range $1 < \Delta q_0 < 1.7$ is necessary for the Hubble diagram method. Stellar evolution requires a correction of similar size and opposite sign; the true q_0 should thus not be far from the formal value.

6. Surface brightnesses, corrected for the effects of dynamical evolution, follow the behavior with redshift expected for relativistic cosmologies. Improved observations may allow measurement of the rate of evolution of the stellar population in galaxies.

7. Galaxy core radii are strongly modified by dynamical effects, but correction for these influences is possible. Such data might be a viable subject for a metric diameter–redshift test, which can provide a useful complement to the Hubble diagram and aid in the elimination of systematic bias in the final results for the deceleration parameter.

I would like to thank J. E. Gunn for much guidance throughout the course of this work. J. Westphal and J. Kristian made available much of their excellent hardware and software. D. Schneider supplied some im-

portant data and provided several extremely useful suggestions regarding the data analysis. Bill Sebok contributed many software suggestions. I thank J. Kristian, J. B. Oke, and S. E. Persson for their very careful criticism of an earlier version of this manuscript. This research was supported in part by NSF grants AST76-22111, AST78-24842, and by NASA contract NAS5-25451.

REFERENCES

Bahcall, N. A. 1977, *Ann. Rev. Astr. Ap.*, **15**, 505.
Baum, W. A. 1972, in *IAU Symposium 44, External Galaxies and Quasi-stellar Objects*, ed. D. S. Evans, (Dordrecht: Reidel), p. 393.
Dressler, A. 1978*a*, *Ap. J.*, **222**, 23.
_____. 1978*b*, *Ap. J.*, **223**, 765.
_____. 1979, *Ap. J.*, **231**, 659.
Geller, M. J., and Peebles, P. J. E. 1972, *Ap. J.*, **174**, 1.
Gudehus, D. H. 1975, *Pub. A.S.P.*, **87**, 763.
Gunn, J. E., and Gott, R. 1972, *Ap. J.*, **176**, 1.
Gunn, J. E., and Oke, J. B. 1975, *Ap. J.*, **195**, 255 (GO).
Gunn, J. E., and Tinsley, B. M. 1976, *Ap. J.*, **210**, 1 (GT).
Hausman, M. A., and Ostriker, J. P. 1978, *Ap. J.*, **224**, 320 (HO).
Hoessel, J. G., Gunn, J. E., and Thuan, T. X. 1980, *Ap. J.*, **241**, 000 (Paper 1).
Hubble, E. P., and Tolman, R. C. 1935, *Ap. J.*, **82**, 302.
Kent, S. M. 1979, *Pub. A.S.P.*, **91**, 394.
King, I. R. 1978, *Ap. J.*, **222**, 1.
Kormendy, J. 1977, *Ap. J.*, **218**, 333.
Kristian, J., Sandage, A., and Westphal, J. A. 1978, *Ap. J.*, **221**, 383.
Oemler, A. 1976, *Ap. J.*, **209**, 693.
Ostriker, J. P., and Hausman, M. A. 1977, *Ap. J. (Letters)*, **217**, L125 (OH).
Ostriker, J. P., and Tremaine, S. D. 1975, *Ap. J. (Letters)*, **202**, L113.
Petrosian, V. 1976, *Ap. J. (Letters)*, **209**, L9.
Rood, H. J., and Leir, A. A. 1979, *Ap. J. (Letters)*, **231**, L3.
Sandage, A. 1961, *Ap. J.*, **133**, 355.
_____. 1972, *Ap. J.*, **178**, 1.
_____. 1976, *Ap. J.*, **205**, 6.
Sandage, A., and Hardy, E. 1973, *Ap. J.*, **183**, 743.
Scott, E. L. 1957, *A.J.*, **62**, 248.
Thuan, T. X., and Gunn, J. E. 1976, *Pub. A.S.P.*, **88**, 543.
Tinsley, B. M. 1976, *Ap. J. (Letters)*, **210**, L49.
Tinsley, B. M., and Gunn, J. E. 1976, *Ap. J.*, **203**, 52 (TG).
White, S. D. M. 1976, *M.N.R.A.S*, **174**, 19.
_____. 1978, *M.N.R.A.S*, **184**, 185.
Young, P. J., Westphal, J. A., Kristian, J., Wilson, C. P., and Landauer, F. P. 1978, *Ap. J.*, **221**, 721.

J. G. HOESSEL: Department of Astronomy, 105–24, California Institute of Technology, Pasadena, CA 91125

PLATE 4

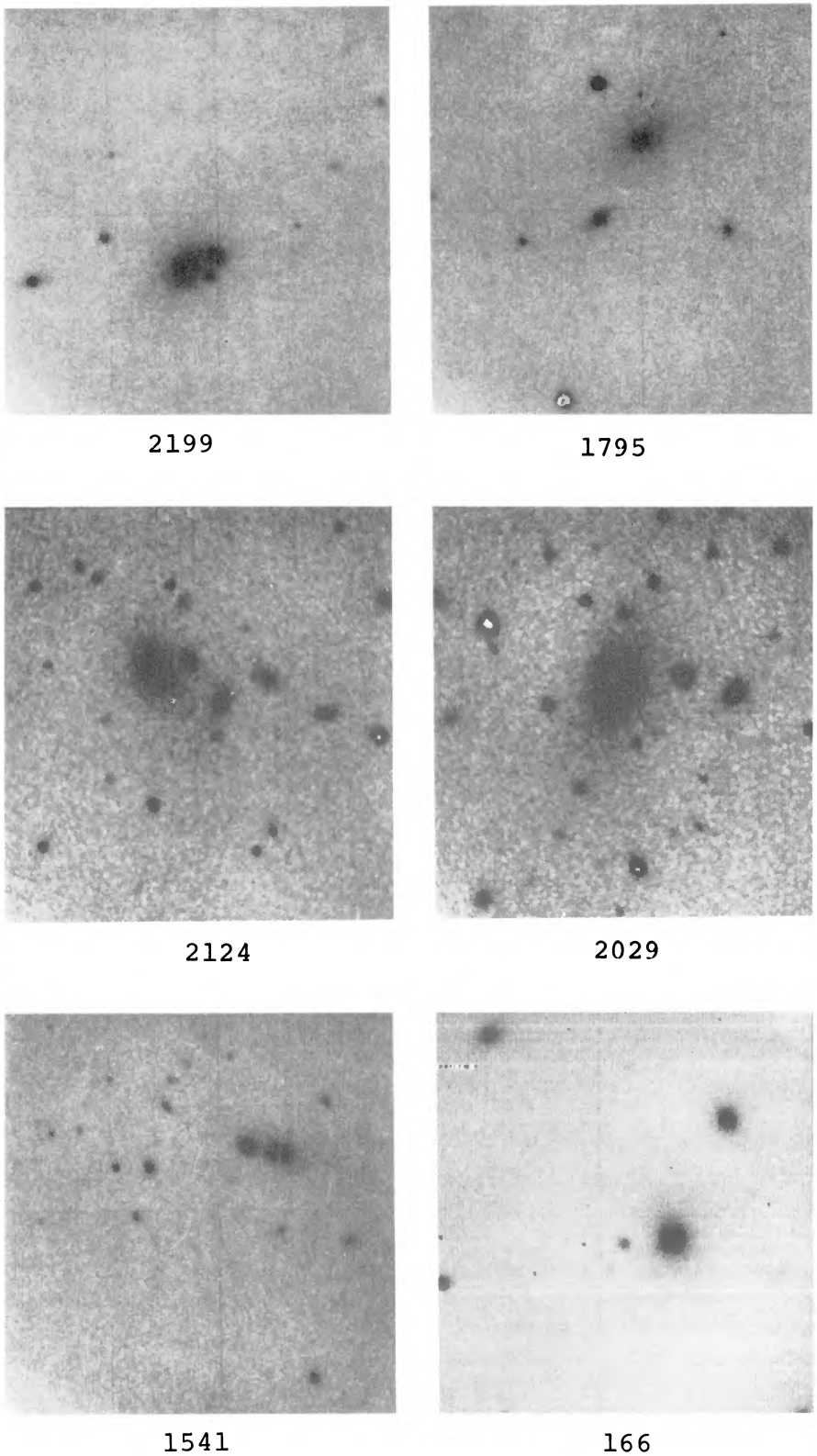

FIG. 1.—Dezeroed and flattened red frames of six galaxies from the sample. The picture of A166 is a CCD frame obtained with the Hale telescope 1′ on a side. The rest are SIT frames 2′ in size made with the 1.5 m telescope. Frames of A2124 and A2029 have been digitally stretched for higher contrast.

HOESSEL (*see* page 494)